Vortex Trajectories and Breakdown on Wing-Canard Configurations

J. Er-El* and A. Seginer†
Technion—Israel Institute of Technology, Haifa, Israel

Flow visualization and force measurement experiments are carried out on close-coupled wing-canard and wing-alone configurations. The effects of the canard sweep angle and longitudinal position on the leading-edge vortex trajectories, their breakdown characteristics, and the configuration aerodynamic coefficients, are studied. The effects of highly (75 deg) and moderately (56 deg) swept canards of equal area are compared. Results show that the canard displaces the leading-edge vortex of the wing upward and outboard in the vicinity of the trailing edge. Increasing the angle of attack results in an upward displacement of these vortices. The angle of attack for which the wing-vortex breakdown points cross the trailing edge on the wing-canard configurations is 8-10 deg higher than in the wing-alone configuration. Increasing the longitudinal separation between the canard and the wing reduces the wing-canard interference. Force measurements show that the normal-force coefficient of the wing—highly-swept-canard configuration at high incidence can be smaller than for the appropriate wing-alone coefficients. This may indicate that the strong leading-edge vortices of the highly-swept canard, which at high incidence are very close to the wing surface near the trailing edge, alter the leeside flow structure there and reduce the lift.

Nomenclature

A = wing area
C_r = wing root chord
C_M = pitching-moment coefficient, $= M/qAC_r$ referred to $\frac{2}{3}C_r$
C_N = normal-force coefficients, $= N/qA$
M = pitching moment referred to $\frac{2}{3}C_r$
N = normal force
q = freestream dynamic pressure
x = longitudinal coordinate aligned with root chord, positive downstream of the wing apex
y = spanwise coordinate relative to wing plane of symmetry
z = vertical coordinate relative to wing surface
α = angle of attack
β = angle between the wing-leading-edge-vortex trajectory at the trailing edge and wing surface (see Fig. 13)

Introduction

THE flowfield about highly swept wings, including delta wings, at moderate to high angles of attack is characterized by the leading-edge vortices. These vortices contribute to the lift by generating low-pressure regions over the wing suction side. This contribution is disrupted when vortex breakdown occurs and the vortex-breakdown stagnation point crosses the wing trailing edge and moves upstream toward the wing apex as the angle of attack is increased. The increased pressures downstream of the vortex-breakdown point and the energy dissipation involved in this process result in a decrease in the lift-curve slope that leads eventually to lift saturation. The increased pressures also cause an increase in the drag and an upstream displacement of the center of pressure.

Although the vortex-breakdown (VBD) process is as yet not fully understood, wing and aircraft designers have developed ways and means to delay its occurrence to higher angles of attack. These include, among others (e.g., double-delta, leading-edge extensions, strakes, etc.), also the close-coupled canard-wing configuration.

The highly nonlinear interaction between the canard and wing could not be evaluated theoretically until the recent development of advanced, nonlinear vortex-lattice methods.[1] The various design features, such as canard geometry, size, and position relative to the wing, in the past were the result of empirical studies.

The aerodynamics of close-coupled wing-canard configurations have been studied experimentally by a number of researchers. Behrbohm[2] studied the effects of the canard position and deflection angle on a generalized aircraft model that consisted of a fuselage, slender wing, and a close-coupled canard. The results were eventually applied to the design of the SAAB-Viggen aircraft. Behrbohm postulated that the canard moved the initial shedding point of the main-wing leading-edge vortices from the apex to a point downstream. Gloss and McKinney[3] and Campbell et al.[4] showed that the vortex lift on another generalized close-coupled-canard aircraft model was proportional to the sweep angle of the canard and nonlinear with respect to its vertical separation. Gloss and Washborn[5] and Hale et al.[6] found that the main-wing loading was reduced by the canard-wing interference at low angles of attack, whereas it was increased at higher incidence.

These experimental results indicate two possible mechanisms by which the canard could affect the flowfield of the wing. One could be the interaction of the canard vortices with the wing leading-edge vortices. The other could be the deflection of the main-wing flowfield by the canard downwash, which should mainly affect the wing-apex region. To verify these mechanisms one has to study the vortex trajectories and the pressure distribution over the wing, with and without a canard.

Vortex trajectories over various wing planforms were determined experimentally by a number of researchers using

Presented as Paper 83-1817 at the AIAA Applied Aerodynamics Conference, Danvers, Mass., July 13-15, 1983; received March 15, 1984; revision received Jan. 31, 1985.

*Lecturer, Department of Aeronautical Engineering.
†Associate Professor, Department of Aeronautical Engineering. Member AIAA.

different methods. Lambourne and Bryer[7] and Erickson[8] obtained such trajectories for wing models in water tunnel tests. In these experiments the vortex cores were visualized by dye injection. Sforza and Smorto[9] and Hummel[10] obtained velocity and pressure maps in the flowfield on the suction side of delta wings and the vortex trajectories could be inferred from their data. Hoeijmakers and Vaatstra[11] obtained vortex trajectories for a 76-deg leading-edge-sweep-angle delta wing and two double-delta wings using a laser-light-sheet technique. However, no data were available for the trajectories of either the wing or the canard vortices on close-coupled canard-wing configurations because they were difficult to measure. Therefore, the purpose of the work described herein is to derive a technique for the determination of these trajectories and to study their dependence on various geometrical parameters of the wing-canard configuration and on its angle of attack. An additional goal was to identify the vortex-breakdown point and determine its spatial position and dependence on the previously mentioned parameters. Finally, an attempt was made to correlate the effects of the canard on the vortex breakdown and vortex trajectories with the variations in the behavior of the configuration's aerodynamic coefficients. Pressure mapping on the surfaces of the same configurations is being performed currently and its results will be published in a subsequent paper.

Experimental Program

Figure 1 features the wing and the two canard models used in the present study. The wing was a flat, 60-deg sweep, delta wing with a sharp leading edge. Two canards were tested in conjunction with the wing. Both were of equal area (approximately 9% of the wing area) but different geometries. One was a highly swept (HS) delta-shaped canard of 75-deg sweep and the other a moderately swept (MS) cropped-arrow-shaped canard of 56-deg sweep. The HS canard was tested on the assumption that its interference with the wing was governed mainly by the interaction of its strong leading-edge vortices with those of the wing. The interference of the MS canard with the wing flowfield was governed by the canard downwash and not by the weaker leading-edge vortices. Thus, both canard-wing interference mechanisms described in the Introduction could be studied. The MS canard was tested at two longitudinal locations relative to the wing to evaluate the influence of the wing-canard separation on their interaction.

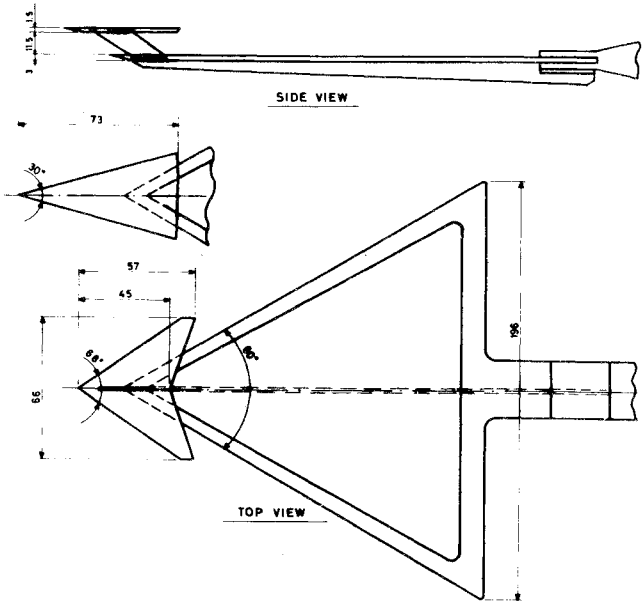

Fig. 1 Wing-MS and -HS canard configurations

The wing-canard configurations tested and the positions of the canards relative to the wing are given in Table 1. The geometries of the wing and MS canard, as well as the canard's location in the rear position, its vertical distance from the wing, and its orientation relative to the wing, were selected to resemble the Kfir-C2 aircraft. The forward position of the MS canard was selected arbitrarily. The position of the HS canard was determined by the (arbitrary) requirement to have its center of pressure coincide with that of the MS canard in its forward position.

The use of a fuselage (resembling the fuselage of the Kfir aircraft) as a mount for both wing and canard was ruled out because of the visualization technique used in this work and described in the following paragraph. Therefore, the canards were mounted on the wing apex via a strut (Fig. 1). A thin (1.5% of wing span) aerodynamically-shaped strut was used to minimize its effects on the flow. A nonintrusive technique had to be used to determine the vortex trajectories because vortex flows are very sensitive even to small disturbances that can alter the investigated phenomenon, especially close to the breakdown point. Therefore, an optical technique was a natural choice. The schlieren flow-visualization method was used because it was simple, inexpensive, and sufficiently sensitive for this purpose. This method senses the density gradient perpendicular to the vortex axis that is the result of the radial pressure gradient in the vortex and the increased axial velocities in the vortex core. Optically, the vortex core with its reduced density is, in effect, a negative cylindrical lens. The parallel rays of the schlieren light beam that is perpendicular to the vortex axis, diverge symmetrically relative to this axis. With the knife edge parallel to the vortex axis the schlieren image of the vortex consists of two regions divided by the core axis: a darker-than-the-background region where the deflected light rays are blocked by the knife edge, and a brighter region where the knife edge

Table 1 Configurations tested and relative positions of the wing and canards

Configuration	Canard position[a]	
	Vertical	Longitudinal
Wing-alone	N/A	N/A
Wing-MS canard, rear position	0.088	0.130
Wing-HS canard	0.088	0.294
Wing-MS canard, forward position	0.088	0.283

[a]The position of the canard apex relative to the wing apex nondimensionalized with respect to the wing root chord.

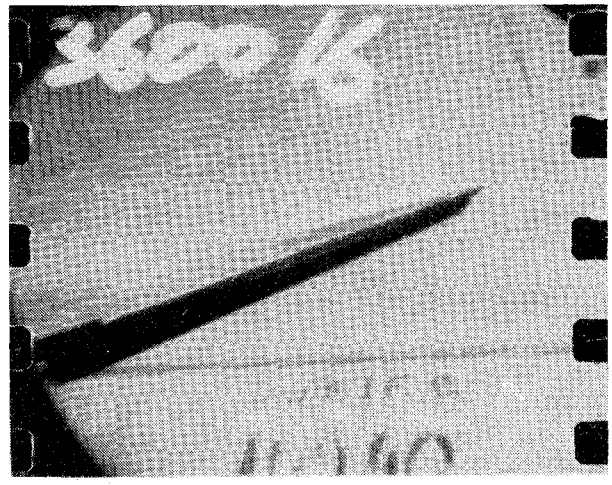

Fig. 2 Schlieren side view of the leading-edge vortices of the wing-alone configuration, $\alpha \cong 17$ deg.

does not block the light rays. The contrast between these regions is sharp and the dividing line is very well defined, even for a wind tunnel speed as low as 60 m/s (~0.2 Mach). This line indicates the trajectory of the vortex axis (e.g., Fig. 2). When vortex breakdown occurs, the radial pressure gradient as well as the axial velocity at the core are reduced considerably. This results in reduced density gradients and the disappearance of the schlieren image of the vortex axis downstream of the vortex breakdown (e.g., Fig. 2).

The visualization of vortex cores by the schlieren technique has been used to study the flow over slender cylindrical bodies[12] and determine the positions of the breakdown points of leading-edge vortices over delta wing.[13] However, it was never used to investigate the vortex trajectories of wing-canard configurations. In the previously mentioned investigations[12,13] only side views of the vortices were presented, i.e., the projection of their trajectories on the pitch plane. Figure 2 is a typical example of such a side view of the present wing-alone configuration at $\alpha \cong 17$ deg. It shows very clearly the trajectory of the wing vortex and its breakdown point. The two-dimensional information contained in this schlieren photograph sufficed for the study of a single vortex. However, the interaction of a pair of vortices, such as the leading-edge vortices of both the canard and wing, including their possible rollup, is a complex three-dimensional phenomenon and its investigation required an additional view of the vortices from a different direction, preferably perpendicular to the wing planform. This was accomplished here by making most of the wing transparent to the schlieren light. The inner part of the wing was made of a clear plastic (Perspex) reinforced by a metal frame (Fig. 3). A thin vertical fin along the root chord on the pressure side (see its projection in Fig. 2) was necessary to increase the stiffness of the wing in the pitch plane. Being on the pressure side, it was estimated that the fin would not interfere with the vortices on the suction side.

All experiments were carried out at a Mach number of 0.2. This velocity was sufficient for the observation of the vortex cores using a schlieren system, yet was sufficiently low to consider the flow as incompressible. The angle-of-attack range covered in these experiments, from about 13 deg to 30 deg, is the region in which the canard effects are more prominent. Side and top view schlieren photographs, as well as force and moment data, were taken as a function of the angle of attack.

The schlieren photographs of the leading-edge vortex images were processed on a film-reader system to obtain vortex trajectories. This was achieved by sampling the coordinates of the boundary line between the dark and bright regions of the image of the vortex core in both the side and top views. The accuracy of the vortex position thus obtained was $\pm 0.002 C_r$. The position of the vortex-breakdown point was determined less accurately (the exact accuracy is difficult to estimate) because the disappearance of the image of the core axis was not sufficiently sharp (e.g., Fig. 2).

Results and Discussion

Typical top and side views of the vortex trajectories at $\alpha \cong 17$ deg on the wing-HS canard and wing-MS canard configurations are presented in Figs. 4 and 5, respectively. Figure 6—the wing-HS canard at $\alpha \cong 24$ deg—is a typical case where vortex breakdown is clearly observed in both the canard and wing vortices. Note that the sections of the wing-leading-edge vortices near the wing apex are not visible in the top views (Figs. 4a and 5a). They are obscured by the opaque, outer frame of the wing. Similarly, the canard vortices cannot be observed over the opaque canard surface (Fig. 4a).

The wing-vortex trajectories, as observed in the schlieren photographs (Figs. 2 and 4-6), are well defined and easily discretized. So also are the vortex trajectories of the HS canard (Figs. 4 and 6). The much weaker vortices of the MS canard are affected by vortex breakdown in the angle-of-attack range studied here and thus are not visible.

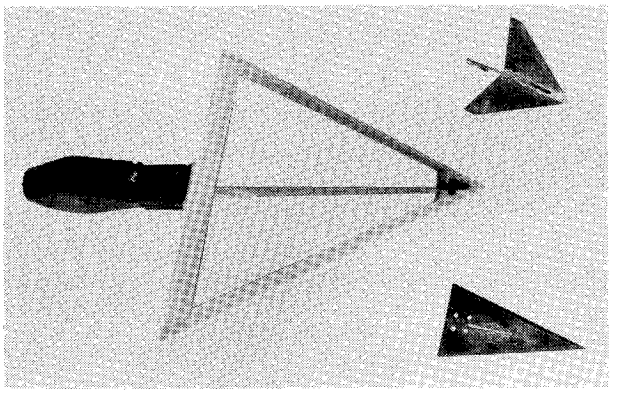

Fig. 3 Photograph of the model.

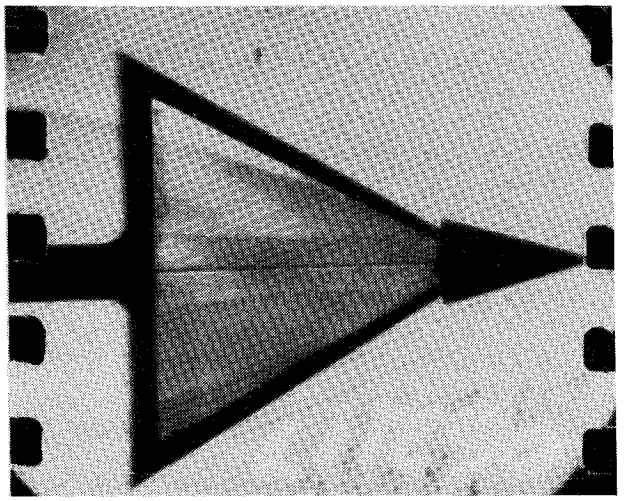

a) Top view.

b) Side view.

Fig. 4 The leading-edge vortices of the wing-HS canard configuration, $\alpha \cong 17$ deg.

Figures 7-10 are the top and side projections of the vortex trajectories of the wing-alone, wing-HS canard, the wing-MS canard in the rear position and the wing-MS canard in the forward position, respectively, at various angles of attack. Also marked on the side projections are the observed vortex-breakdown points. The vertical coordinate in the side projections is stretched in order to improve their readability. Consequently, the vortex trajectories in the side views appear more widely spread than in reality. Note that the wing vortices are shed at the wing apex, but their trajectories can be measured only after they clear the wing frame.

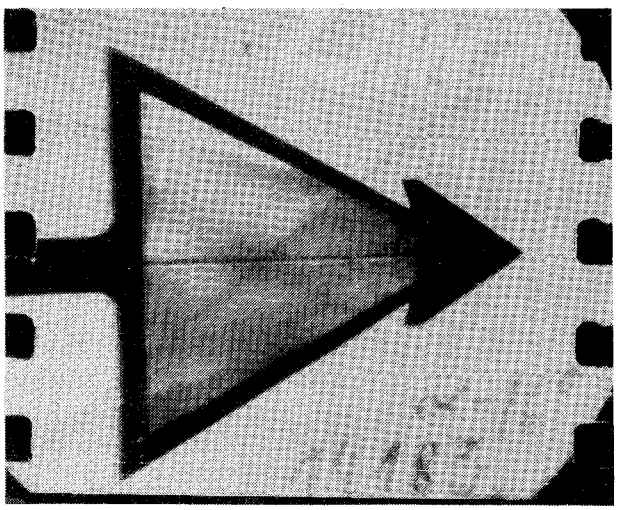

a) Top view.

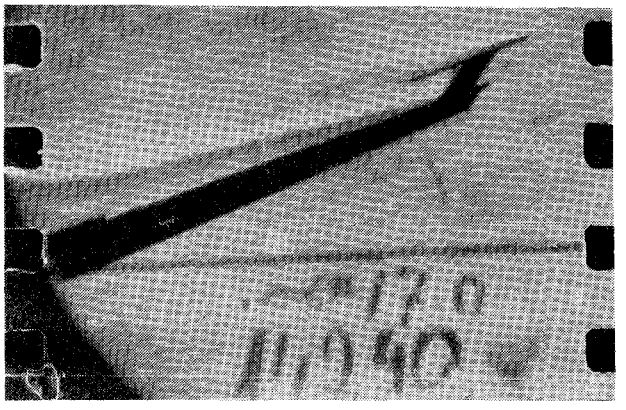

b) Side view.

Fig. 5 The leading-edge vortices of the wing-MS canard (rear position) configuration, $\alpha \cong 17$ deg.

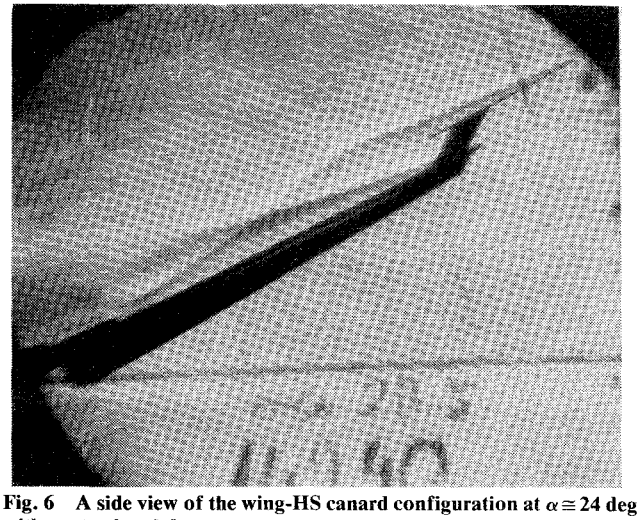

Fig. 6 A side view of the wing-HS canard configuration at $\alpha \cong 24$ deg with vortex breakdown.

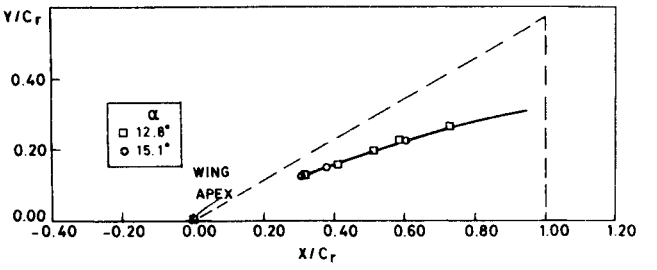

a) Spanwise component.

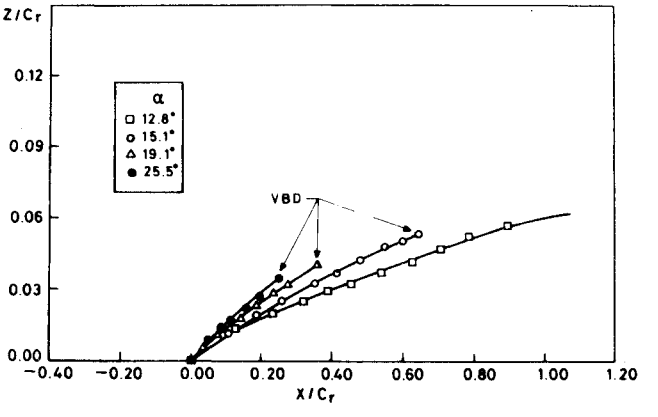

b) Vertical component.

Fig. 7 Leading-edge vortex trajectories, wing-alone configuration.

Interaction of Wing-Canard Leading-Edge Vortices

Effects of the Canard on the Vortex Trajectories

Two different mechanisms, by which the canard influences the trajectories of the wing vortices, were hypothesized in the Introduction. Near the wing apex, in the near wake of the canard, its downwash as a lifting surface (of the "bound" vortex) is the dominant feature of the flowfield. Such a mechanism forces the wing vortices down, closer to the wing surface. This can be seen by comparing Fig. 7 with Figs. 8-10. Plotting all of the side projections for all of the configurations at $\alpha \cong 19$ deg on one figure (Fig. 11) further accentuates this observation. Furthermore, it is evident from this figure that the MS canard, which generates more lift than the HS canard because of its higher aspect ratio, induces a larger downward displacement.

Further downstream the vortex trajectories are more influenced by the canard leading-edge vortices than by its lift-related downwash. A schematic arrangement of the locations of the various vortices and the directions of the resultant mutually induced velocities and displacements is presented in Fig. 12. As long as the canard vortices are inboard of the wing vortices they induce on them an upward displacement relative to the wing-alone vortex position. This is substantiated by Fig. 11. The combined effect of the canard downwash near the wing apex and the upwash of the canard vortices further downstream bends the wing vortices into an upward concave trajectory (Fig. 11), whereas the original trajectory on the wing-alone configuration was upward convex. This change in curvature is quite evident in Figs. 8b, 9b, and 10b for angles of attack higher than ~15 deg, as compared with the vortex trajectories of the wing-alone configuration (Fig. 7b). It is interesting to note that the weaker vortices of the higher-aspect-ratio canard (Figs. 9b and 10b) have the same effect as those of the highly swept canard (Fig. 8b) despite their early breakdown. This corroborates existing experimental evidence[17] that the circulation in a vortex is not reduced considerably by the vortex breakdown and, therefore, can induce velocities of the same order as those induced by a vortex unaffected by vortex breakdown.

Assuming that the canard vortices are always inboard of the wing vortices beause of the smaller span of the canard and its upstream position (Figs. 4a, 5a, and 8a), they also will induce an outboard displacement (Fig. 12) on the wing vortices when

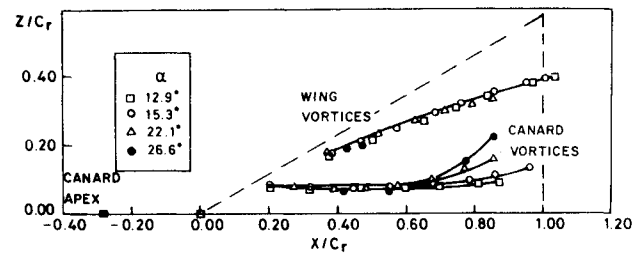

a) Spanwise component.

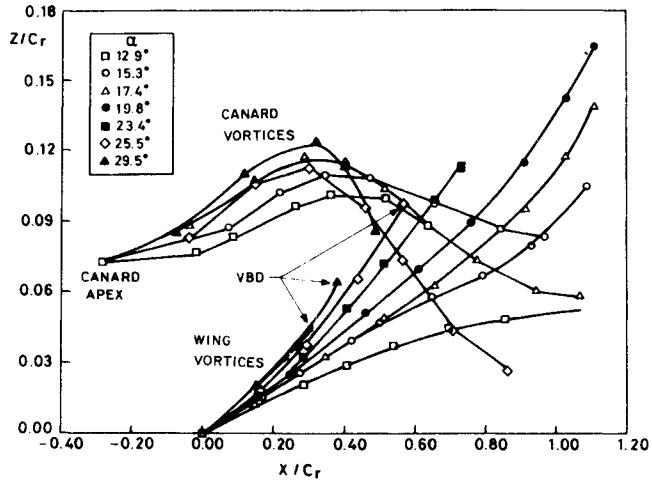

b) Vertical component.

Fig. 8 Leading-edge vortex trajectories, wing-HS canard configuration.

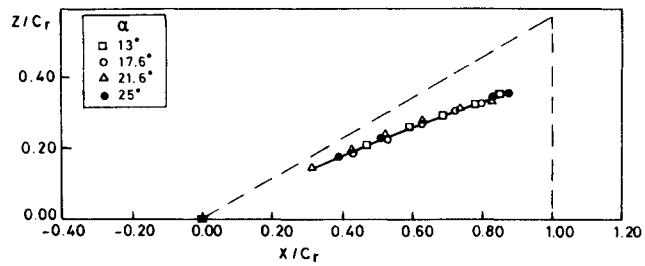

a) Spanwise component.

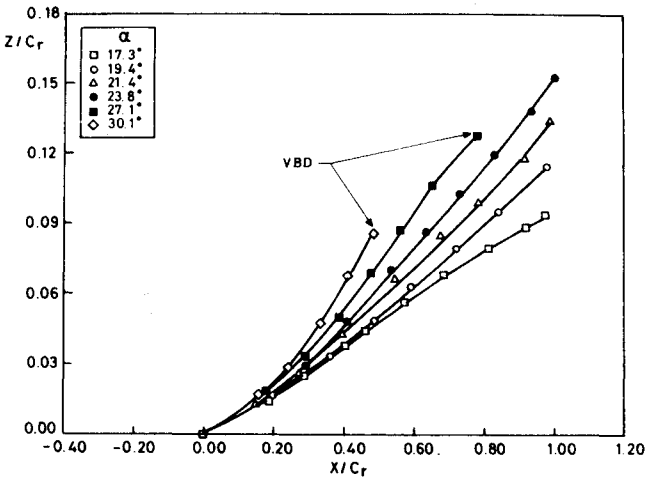

b) Vertical component.

Fig. 9 Leading-edge vortex trajectories, wing-MS canard, in rear position.

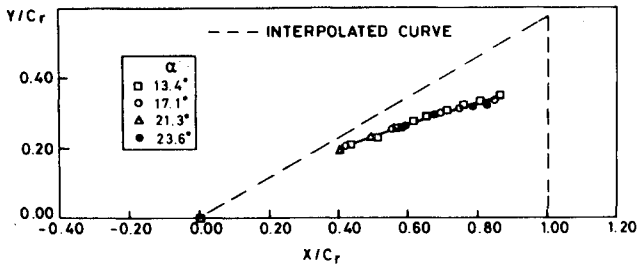

a) Spanwise component.

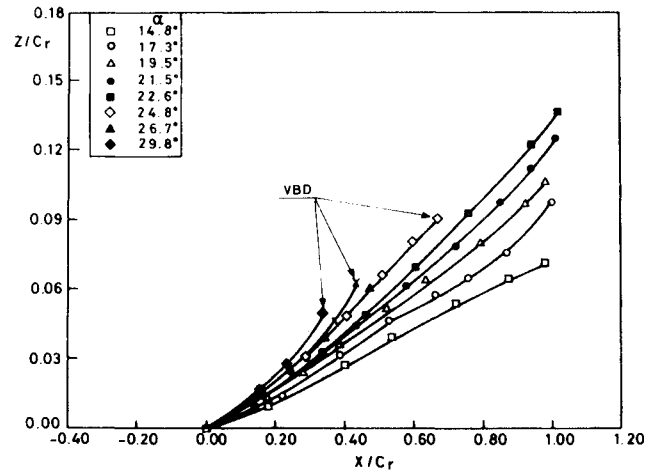

b) Vertical component.

Fig. 10 Leading-edge vortex trajectories, wing-MS canard, in forward position.

they are above them (compare Fig. 7a with Figs. 8a, 9a, and 10a). A measure of this outward displacement of the vortices is the spanwise distance between the two leading-edge vortices of the wing where they cross its trailing edge—approximately $0.80C_r$ for the wing-HS canard configuration, $0.78C_r$ and $0.74C_r$ for the configuration with the MS canard in the rear and forward positions, respectively, and 0.55 for the wing alone. The spanwise distances between the vortices vary only slightly when the angle of attack is changed, and the values presented here are averaged over the angle-of-attack range.

The sliding scale in the canard-induced spanwise displacement of the vortices relative to their positions on the wing-alone configuration is indicative of a corresponding weakening of the canard effects. The largest displacement is induced by the strong vortices of the HS canard. Increasing the longitudinal separation between the MS canard and the wing results in a reduced spanwise displacement (as indicated in the previous paragraph). It is also accompanied by a smaller downward displacement in the apex region and a smaller upward displacement in the vicinity of the trailing edge (Figs. 9 and 10). This indicates that the wing-canard interference decreases with increasing longitudinal separation, both due to the reduced area over which the canard-induced downwash affects the wing and to the longer distance between the wing and canard vortices and their resultant reduced interaction.

Increasing the angle of attack results in an upward displacement of the wing vortices with respect to the wing surface for all of the configurations (Figs. 7b-10b). The corresponding spanwise displacement of these vortices, in the incidence range studied here, is of the order of the resolution of the schlieren photograph and the film reader. Therefore, no conclusion can be drawn as to its trend (Figs. 7b-10b). Similar trends have been predicted by the analytical models of Brown and Michael[14] and Smith[15] for delta wings. A small ratio of spanwise-to-vertical displacement has also been observed on a delta wing model of aspect ratio 1.0 (76 deg sweep).[10]

The vertical position of the wing vortices at the trailing edge also is indicative of wing-canard interference. This position is represented by the angle β as defined in Fig. 13. This angle is also used as a first approximation of the vortex-trajectory orientation by various nonlinear lift theories (e.g., Ref. 16). The present results show (Fig. 13) that this angle increases when the angle of attack is increased. At a given angle of attack the wing-HS canard configuration usually produces the largest value of β and the wing-MS canard configuration in the forward position produces the smallest value. One can conclude, on the basis of Fig. 13, that the rate of increase of β with respect to the angle of attack, $(d\beta/d\alpha)$, is approximately 0.5 and is consistent with the slope of Gersten's relation[16] $\beta=\alpha/2$ but the actual values are lower (Fig. 13). An average straight line through the experimental results intersects the α axis at $\alpha\cong 6$ deg, the approximate angle at which the wing begins to shed the leading-edge vortices.

The leading-edge vortices of the HS canard itself are displaced outboard (Fig. 8a) as a result of an increasing angle of attack. Their vertical displacement is upward near the apex, apparently due to the main-wing upwash, and downward at the trailing edge due to the wing-vortices downwash. Consequently, the curvature of these trajectories is increased (see Fig. 8b).

Canard Effects on Vortex Breakdown

Figure 14 presents the position of vortex breakdown of the wing leading-edge vortices as observed by schlieren photography. Generally speaking, within the accuracy of determining the position of the vortex-breakdown point from the schlieren picture, there are no significant differences between the results of all three wing-canard configurations. The vortex-breakdown point crosses the trailing edge at an angle of attack of about 22-24 deg for the wing-canard configuration, compared with 14 deg for the wing alone. This difference of about 8-10 deg also prevails when the breakdown point moves upstream as the angle of attack is increased.

There is a good agreement between the vortex-breakdown position for the wing-alone configuration and the data obtained by Wentz and Kohlman[13] for a 60-deg-sweep delta wing. The sensitivity of the vortex-breakdown position to changes in the angle of attack is high when the breakdown is near the trailing edge; i.e., an increase in the angle of attack of about 2 deg moves the breakdown point upstream to about 60% of the chord length. This high sensitivity was manifested in these tests as an instability in the vortex-breakdown position. As a result, stable vortex-breakdown readings in the trailing-edge region were unobtainable.

Force and Moment Measurements

The force and moment data taken during the flow visualization were reduced to aerodynamic coefficients. Figure 15 features curves of the normal-force and pitching-moment coefficients. The normal-force curves of the wing-canard configurations have a similar trend in the range from the lowest angle of attack tested to about 24 deg, the angle at which vortex breakdown first occurs over the trailing edge on the

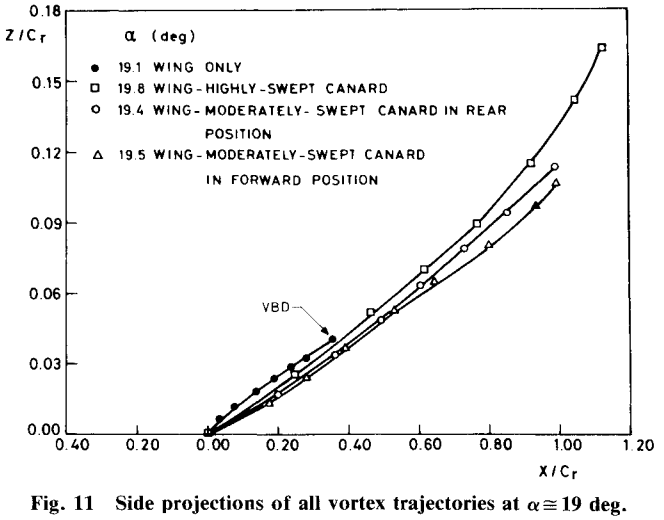

Fig. 11 Side projections of all vortex trajectories at $\alpha\cong 19$ deg.

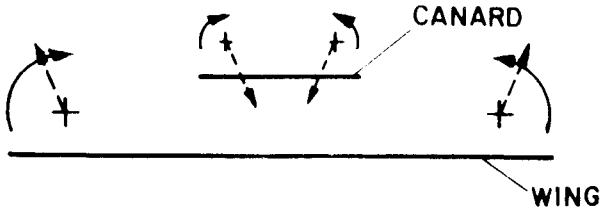

Fig. 12 Schematic rear view of mutually induced displacements of the wing and canard vortices.

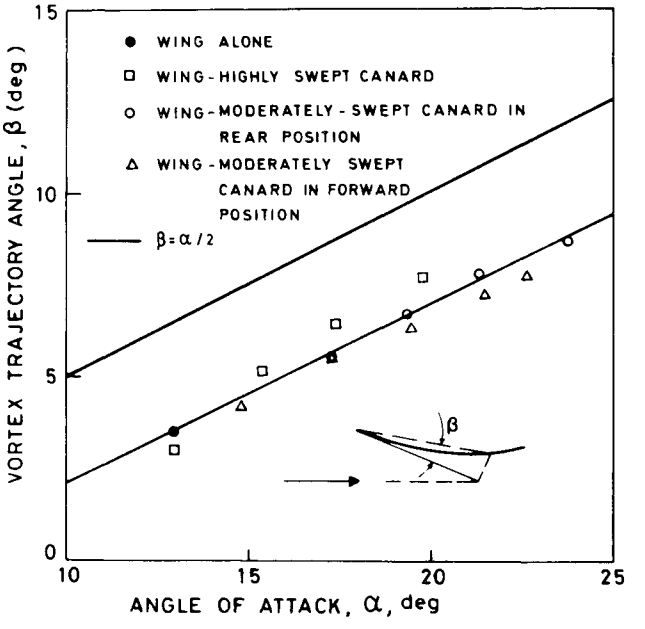

Fig. 13 The vortex-trajectory angle at the trailing edge as a function of angle of attack.

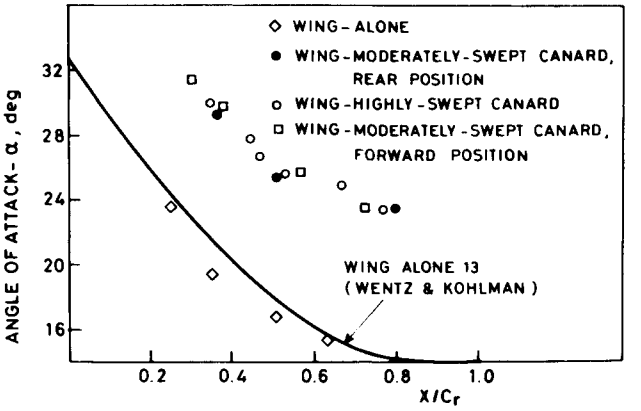

Fig. 14 Longitudinal position of vortex breakdown.

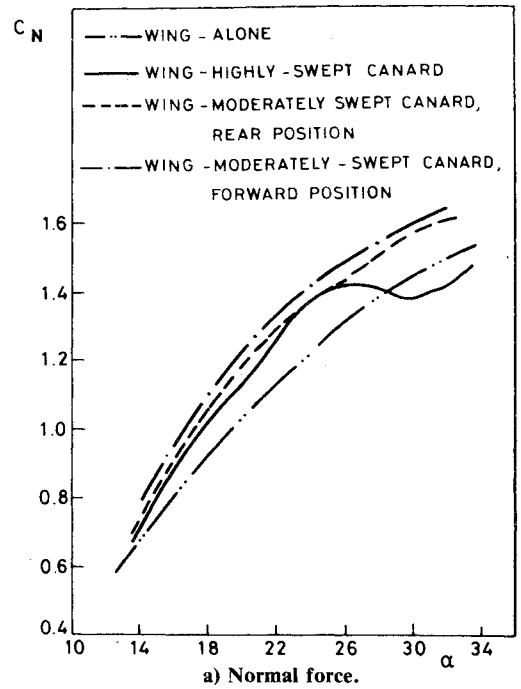

a) Normal force.

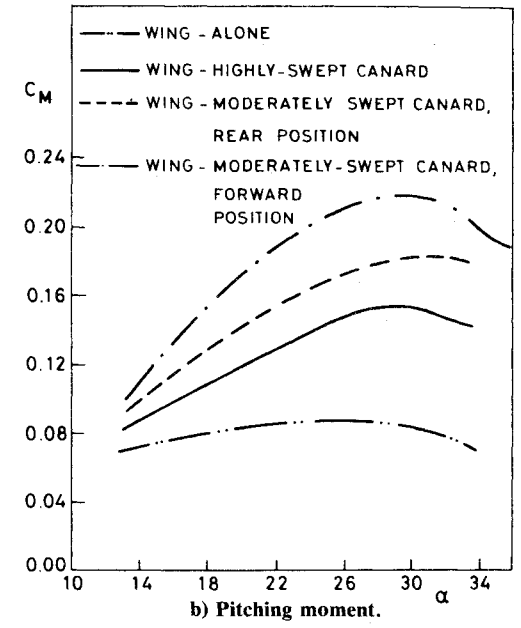

b) Pitching moment.

Fig. 15 Normal-force and pitching-moment coefficients.

wing-HS canard configuration. In the 24 deg $\leq \alpha \leq$ 30 deg range, the slope of C_N changes from positive to negative with increasing incidence for this configuration. This decrease results in a local maximum of C_N at $\alpha \cong 26$ deg, and in smaller C_N values than those of the wing alone for $\alpha > 28$ deg. A possible explanation for this behavior is offered in the Summary. Comparison of the two C_N curves of the wing-MS canard configurations reveals that C_N increases with increasing longitudinal separation, probably due to decreasing vortex interference. The addition to the normal force due to the presence of the canard at $\alpha \cong 22$ deg is about 18% and 15% for the configurations with the MS canard in the forward and rear positions, respectively. This indicates that the contribution of the canard to C_N at this angle of attack is considerably larger than the addition of about 9% to the wing area.

The pitching-moment coefficients of all of the configurations tested increase monotonically up to the angle-of-attack range of 25-30 deg (Fig. 15b). The variation in C_M of the wing-alone case is small compared with the variations in the pitching-moment coefficients of the wing-canard configurations. The configuration with the MS canard in the forward position has a higher pitching moment than with the canard in the rear position, probably because of the canard's longer moment arm.

Summary and Conclusions

A close-coupled canard placed upstream and above a 60-deg delta wing causes a delay in the onset of vortex breakdown of the wing leading-edge vortices, as well as a downward displacement of their trajectories in the wing apex region, and an upward displacement near the trailing edge. There is no simple explanation for the abovementioned delay, primarily because vortex breakdown itself, and the conditions for its onset on leading-edge vortices, are not sufficiently known. Based on the results reported here, the delay can be reasoned as follows: the upward displacement of the leading-edge vortices of the wing near the trailing edge should be accompanied by an increase in their circulation. Such an increase is necessary to maintain equilibrium in their new positions, as has been predicted by analytical models of vortex flow over delta wings.[14,15]

The combination of the increased circulation and the increased vertical separation of these vortices from the leading edge, which also removes them from the adverse pressure gradients that develop near the trailing edge of the wing, results in their increased stability. However, this does not explain the difference between the normal-force characteristics of the wing-HS canard and those of wing-MS canard configurations in the post-vortex-breakdown range, which is quite large although neither their vortex-breakdown curves nor their vortex trajectories differ significantly.

The reduction in the normal force of the wing-HS canard configuration in the 24-30-deg incidence range indicates a pressure rise on the leeside of the wing. Since the trajectories and the breakdown characteristics of the wing leading-edge vortices of this configuration are similar to those of the wing-MS canard configuration (which does not exhibit a similar decline in the lift), it may be assumed that the difference is due to the different behavior of the canard vortices of the two configurations. The vortices of the HS canard almost touch down at the trailing edge on the leeside of the wing and their induced velocities may alter the structure of the flowfield above the wing to produce the higher pressures mentioned previously.

A study of the pressures on the leeside surface of the wing and flowfield over it is, therefore, needed to improve the understanding of wing-canard interference and its effect on the aerodynamics of the configuration. However, it is evident that although all of the canards postponed the vortex breakdown from $\alpha \cong 14$ deg to $\alpha \cong 22$-24 deg, the wing canard interference does not necessarily result in improved aerodynamic characteristics. Furthermore, the results here indicate that the weakest interference was the best as far as lift was concerned.

The angle (β), which is a rough approximation for the orientation of the leading-edge vortices relative to the wing surface, was found to be smaller than the $\alpha/2$ relation used by Gersten[16] and others. However, the rate at which this angle increases with an increase in the angle of attack is approximately 0.5 in the experiments described herein, and is in agreement with Gersten's relation ($\beta \cong \alpha/2$). Therefore, this relation should be modified in accordance with the present data to account for the fact that leading-edge vortices start shedding at the wing apex at about $\alpha \cong 6$ deg. A better correlation with the experimental results is obtained with $\beta = \frac{1}{2}(\alpha - 6)$, where β and α are given in degrees.

Acknowledgment

The authors would like to acknowledge the helpful discussions with Prof. A. Sigal during the preparation of this manuscript.

References

[1]Rusak, Z., Wasserstrom, E., and Seginer, A., "Numerical Calculation of Nonlinear Aerodynamics of Wing-Body Configurations," *AIAA Journal,* Vol. 21, July 1983, pp. 929-936.

[2]Behrbohm, H., "Basic Low Speed Aerodynamics of the Short Coupled Canard Configuration of Small Aspect Ratio," SAAB Aircraft Co., Linkoping, Sweden, SAAB TN-60, July 1965.

[3]Gloss, B. B. and McKinney, L. W., "Canard-Wing Lift Interference Related to Maneuvering Aircraft at Subsonic Speeds," NASA TMX-2897, Dec. 1973.

[4]Campbell, J. F., Gloss, B. B., and Lamar, J. E., "Vortex Maneuver Lift for Supercruise Configurations," NASA TMX-72836, Feb. 1976.

[5]Gloss, B. B. and Washborn, K. E., "A Study of Canard-Wing Interference Using Experimental Pressure Data at Transonic Speeds," NASA TP-1355, Jan. 1979.

[6]Hale, R. W., Tan, P., and Ordway, D. E., "Predictions of Aerodynamic Loads on Close-Coupled Canard Configurations—Theory and Experiments," Sage Action Inc., Ithaca, N.Y., SAI-AR-7702, July 1977.

[7]Lambourne, N. C. and Bryer, D. W., "The Bursting of Leading-Edge Vortices—Some Observations and Discussion of the Phenomenon," Aeronautical Research Council, Great Britain, RM-3282, April 1961.

[8]Erickson, G. E., "Flow Studies of Slender Wing Vortices," AIAA Paper 80-1423, July 1980.

[9]Sforza, P. M. and Smorto, M. J., "Streamwise Development of the Flow Over a Delta Wing," AIAA Paper 80-0200, Jan. 1980.

[10]Hummel, D., "On the Vortex Formation Over a Delta Wing at Large Angles of Incidence," AGARD CP-247, Oct. 1978.

[11]Hoeijmakers, H.W.M. and Vaatstra, W., "On the Vortex Flow Over Delta and Double-Delta Wings," AIAA Paper 82-0949, June 1982.

[12]Thomson, K. D. and Morrison, D. F., "The Spacing Position and Strength in the Wake of Slender Cylindrical Bodies at Large Incidence," *Journal of Fluid Mechanics,* Vol. 50, March 1971, pp. 751-783.

[13]Wentz Jr., W. H. and Kohlman, D. L., "Wind Tunnel Investigations of Vortex Breakdown on Slender Sharp-Edged Wings," University of Kansas Center for Research, Lawrence, Kans., Rept. FRL 69-013, Nov. 1968.

[14]Brown, C. E. and Michael, W. H., "Effects of Leading-Edge Separation on the Lift of a Delta Wing," *Journal of the Aeronautical Sciences,* Vol. 21, Oct. 1954, pp. 690-694.

[15]Smith, J. H. B., "Improved Calculations of Leading-Edge Separation from Slender Delta Wings," RAE TR-66070, March 1966.

[16]Gersten, K., "A Nonlinear Lifting Surface Theory for Low Aspect-Ratio Wings," *AIAA Journal,* Vol. 1, April 1963, pp. 924-925.

[17]Garg, A. K. and Leibovich, S., "Spectral Characteristics of Vortex Breakdown Flowfields," *The Physics of Fluids,* Vol. 22, Nov. 1979, pp. 2053-2069.